Individual pitch controller with static inverted decoupling for periodic blade load reduction on monopile offshore wind turbines

Lara, Manuel; Ruz, Mario L.; Mulders, Sebastiaan Paul; Vázquez, Francisco; Garrido, Juan

DOI
10.1016/j.oceaneng.2025.121608

Publication date
2025

Document Version
Final published version

Published in
Ocean Engineering

Citation (APA)
Lara, M., Ruz, M. L., Mulders, S. P., Vázquez, F., & Garrido, J. (2025). Individual pitch controller with static inverted decoupling for periodic blade load reduction on monopile offshore wind turbines. *Ocean Engineering*, *334*, Article 121608. https://doi.org/10.1016/j.oceaneng.2025.121608

Ocean Engineering 334 (2025) 121608

Contents lists available at ScienceDirect

Ocean Engineering

journal homepage: www.elsevier.com/locate/oceaneng

Research paper

Individual pitch controller with static inverted decoupling for periodic blade load reduction on monopile offshore wind turbines

Manuel Lara [a,*], Mario L. Ruz [b], Sebastiaan Paul Mulders [c], Francisco Vázquez [a], Juan Garrido [a]

[a] Department of Electrical Engineering and Automation, University of Cordoba, Campus of Rabanales, 14071, Cordoba, Spain
[b] Department of Mechanics, University of Cordoba, Campus of Rabanales, 14071, Cordoba, Spain
[c] Delft Center for Systems and Control, Faculty of Mechanical Engineering, Delft University of Technology, Mekelweg 2, 2628 CD, Delft, the Netherlands

ARTICLE INFO

Keywords:
Wind turbine control
Offshore wind turbine
Fatigue load mitigation
individual pitch control
decoupling control
genetic algorithms

ABSTRACT

Individual pitch control (IPC) is a technique used to reduce periodic blade loads in wind turbines. It generally uses the multiblade coordinate transformation to convert blade load measurements from a rotating frame into a two-axes non-rotating frame. Although these non-rotating axes are assumed to be decoupled, studies reveal persistent interactions. Reducing this coupling, such as by introducing an azimuth offset, enhances IPC performance. This study explores the impact of static inverted decoupling, which decouples the process in the steady state, on IPC performance. The proposed IPCs are adaptive, scheduling controller and decoupling gains based on operational conditions. In such IPC designs, the integral gains of the diagonal controllers and the decoupling elements can either be the same or different. These methods were validated on a simulated 15 MW wind turbine. Controller parameter optimization was accomplished through genetic algorithms to minimize blade fatigue loads, measured via the damage equivalent load (DEL). Results indicate that incorporating static inverted decoupling into IPC improves blade load reduction without increasing pitch actuator effort. IPCs with similar integral gains and matching absolute values in decoupling elements achieved the best balance between DEL reduction and complexity with minimal actuator effort, while additional optimization parameters provided negligible improvements.

1. Introduction

Offshore wind energy has experienced exponential growth in the last decade, with a global installed capacity of 64.3 GW in 2022, representing 7.1 % of global wind capacity (Williams and Zhao, 2023). This growth is due to the need to diversify energy sources and reduce greenhouse gas emissions. Currently, large-capacity wind turbines with fixed monopile foundations represent the dominant technology in offshore wind energy (Musial et al., 2023), (Kapasakalis et al., 2024). The increase in the rotor size and generating capacity of wind turbines has brought significant challenges (Energy, 2021), (Patro et al., 2024). Aspects such as operational stability, safety, and vibration control have aroused increasing interest in the scientific community (Veers et al., 2023), requiring the study of advanced control strategies to manage structural loads and ensure optimal performance in adverse environmental conditions.

Wind turbines operate in four main regions (Muñoz-Palomeque et al., 2024), each with specific characteristics and control requirements. In the full load region (Region III), where the wind speed exceeds the rated speed, collective pitch control (CPC) is used to regulate the rotor speed and limit the power generated (Lasheen et al., 2020), (El Yaakoubi et al., 2023). However, CPC is not sufficient to mitigate the asymmetric loads acting on the blades, which has led to the development of individual pitch control (IPC) (Bossanyi, 2003). IPC has become a key strategy to reduce the fatigue loads on the blades, especially harmonic loads (El Yaakoubi et al., 2023). Using multiblade coordinate (MBC) transformation (Routray et al., 2023), IPC converts blade rotation signals to a fixed reference system, enabling the design of single-input-single-output (SISO) controllers (Bossanyi et al., 2013).

Despite its advantages, traditional IPC faces challenges due to the dynamic coupling between the tilt and yaw axes, which limits its effectiveness (Geyler and Caselitz, 2008). Traditional IPC methods use simple linear SISO controllers (El Yaakoubi et al., 2023), (Minh Le et al., 2019), not always achieving effective decoupling between the tilt and

* Corresponding author.
E-mail address: p12laorm@uco.es (M. Lara).

https://doi.org/10.1016/j.oceaneng.2025.121608
Received 6 March 2025; Received in revised form 2 May 2025; Accepted 17 May 2025
Available online 23 May 2025

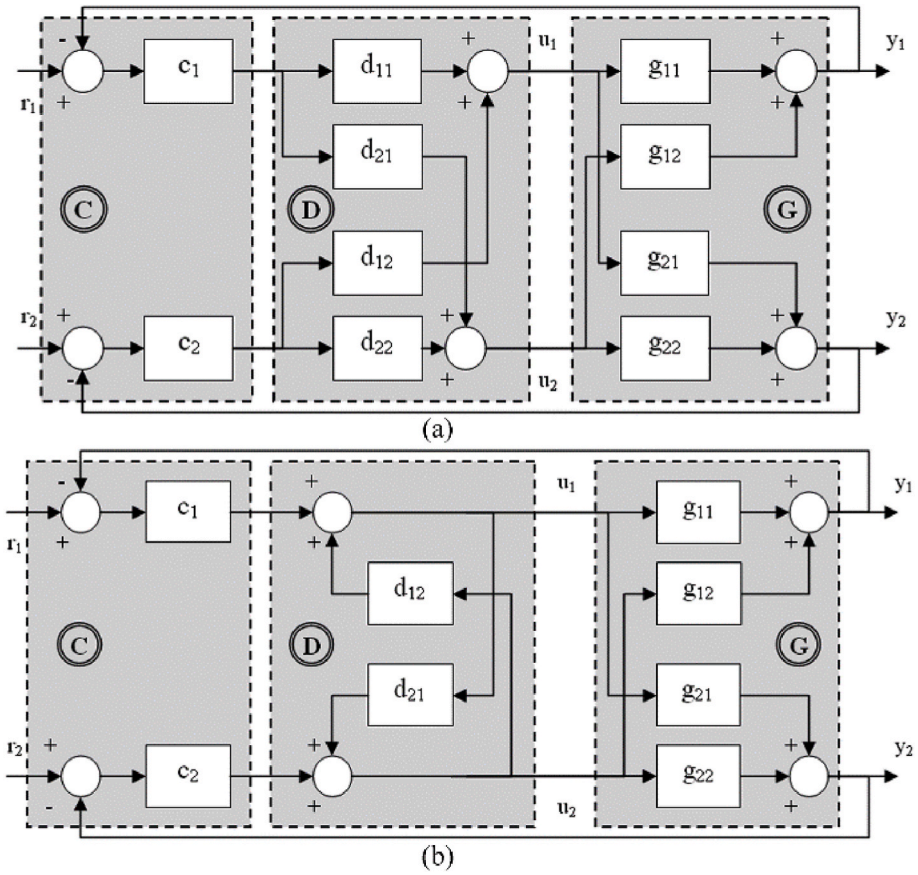

Fig. 1. Decoupling network approaches: a) conventional decoupling, b) inverted decoupling.

yaw dynamics (Geyler and Caselitz, 2008). This can result in unexpected behaviors under different wind and turbulence conditions, which has motivated the study of multivariable control methods, that better accounts for the complex interactions between the system dynamics. Multivariable control methods have been applied for years to various aspects of wind turbine control. This field is the subject of active interest, as evidenced by several studies that have developed different multivariable control methodologies. These methodologies range from traditional decentralized PID controllers (Wu et al., 2008) to more sophisticated techniques, such as model-based predictive control (Yang et al., 2007), robust H_∞ control (Lasheen et al., 2020), and nonlinear control (Boukhezzar et al., 2007). Concrete examples of multivariable controllers in the IPC can be found in (Vali et al., 2016), (Yuan et al., 2020). In recent years, work has been done using different optimization methods for IPC (Aktan and Bottasso, 2023), (Mulders et al., 2020), (Lara et al., 2023) that allow improving the controller performance by minimizing fatigue loads and adapting to varying wind conditions. Since the tuning of IPC controllers is a complex process due to the highly dynamic nature of wind turbines, where wind characteristics are constantly changing, there are studies that propose the use of genetic algorithms for controller tuning in wind turbines (Rasekh and Aliabadi, 2023).

Among the multivariable control methods are the decoupling strategies, which allow obtaining a decoupling in multivariable systems and are relatively easy to design and implement (Garrido et al., 2011). In (Ungurán et al., 2019) a static decoupling based on the inverse of the steady-state gain matrix of the process is used in the IPC to decouple the system at low frequencies and improve control performance. In (Mulders et al., 2019), authors proposed the inclusion of an azimuth offset in the inverse MBC transformation to decouple the system and demonstrated that it is similar to a normalized version of the steady-state gain matrix of the inverse plant.

Most decoupling network approaches are implemented using a conventional scheme where the decoupling network and its elements are equivalent to a matrix and its elements. In them, the control signals are obtained through a weighted combination of the decentralized controller outputs, but the scheme has several practical problems for its implementation (Garrido et al., 2011). Inverted decoupling is an alternative scheme for implementing decoupling networks that derives the control signals as a combination of one decentralized controller output and the other control signals. Fig. 1 shows both decoupling approaches for 2×2 processes, where g_{ij} are the process transfer functions, d_{ij} are the decoupling elements, c_i are the decentralized controllers, y_i are the controlled variables, u_i are the control signals, and r_i are the references (Garrido et al., 2011). The inverted structure offers several advantages over other types of conventional decoupling. For example, it allows maintaining apparent processes similar to the original processes with simple decoupling elements (Garrido et al., 2011). In addition, it has important practical implementation advantages, as extensively investigated in (Garrido et al., 2011). In (Hägglund et al., 2022), static inverted decoupling is proposed to be applied to previous decentralized controllers that are designed only considering the diagonal process elements. The static decoupling elements are calculated from the process steady-state gain matrix. The interaction is reduced, although due to the gain introduced by the static inverted decoupling, the authors proposed to retune the decentralized controller gains using a correction factor equal to $(1\text{-}d_{12}d_{21})$ in order to maintain the gain of the original control design.

In our previous study (Lara et al., 2024), we showed how dynamic inverted decoupling implemented in IPC can improve wind turbine performance by reducing interactions, thereby outperforming traditional IPC strategies. The main objective of this study is to analyze the

performance improvement provided by the inclusion of optimal static inverted decoupling compared to the traditional decentralized IPC scheme. To carry out a fair comparison, the parameters of the different schemes were optimized with the objective of minimizing the fatigue in out-of-plane (OoP) blade loads according to the damage equivalent load (DEL) (Ragan and Manuel, 2007), thus ensuring impartiality in the evaluation process. The proposed schemes were applied to the International Energy Agency (IEA) 15 MW reference wind turbine. Due to the nonlinearity of the system and its variation with wind speed, the proposed IPC schemes were implemented as adaptive controllers with gain scheduling within the nominal region. The main novelties of this work compared to the available literature are the following.

- Static inverted decoupling in IPC: to the best of our knowledge, there is no research prior to the one carried out by the authors in their previous work (Lara et al., 2024), where the improvement of the existing interaction in IPC control loops by means of static inverted decoupling is addressed. Here, different combinations of such decoupling with the traditional IPC were studied and the improvements that can be achieved with them to minimize the fatigue load on the blades have been analyzed qualitatively and quantitatively.
- Adaptive IPC: the proposed IPC schemes were implemented as adaptive blocks where the controller gains and decoupling elements were adapted according to the mean value of the measured filtered blade moments, rather than based on the wind speed.
- Research on larger capacity turbines: most of the IPC research papers published to date have focused on the NREL 5 MW wind turbine. However, this study was conducted on the IEA 15 MW wind turbine, which is more relevant according to current sizes of offshore wind turbines.

The results show that the inclusion of the static inverted decoupling in the IPC achieves a greater reduction in the blade fatigue loads, using a pitch actuation effort similar to the traditional IPC. The article is organized as follows: Section 2 introduces the background on IPC, Section 3 presents the methodology including the decoupling element design and parameter tuning, Section 4 provides a comparative analysis of the proposed controllers, and Section 5 details the conclusions and future research.

2. Background on individual pitch control

Individual Pitch Control (IPC) is a technique widely used in wind turbine control systems to mitigate the periodic loads experienced by the blades, particularly 1P (once per revolution) harmonic loads (Van Engelen, 2006). These loads arise due to blade rotation and are influenced by factors such as wind shear, turbulence, and tower shadow. IPC works by independently adjusting the pitch angle of each blade based on real-time load measurements, thus reducing the asymmetric loads that contribute to fatigue damage.

The core of IPC lies in the multiblade coordinate (MBC) transformation that converts the bending moments at the root of each blade from a rotating reference frame (associated with each blade) to a fixed (non-rotating) reference frame. This allows the control system to target specific load components. The MBC transformation maps the bending moments at the root of the blades from the rotating reference frame to the fixed frame. For a 3-bladed wind turbine, the transformation is defined as

$$\begin{bmatrix} M_t(t) \\ M_y(t) \end{bmatrix} = \mathbf{T}(\psi) \begin{bmatrix} M_1(t) \\ M_2(t) \\ M_3(t) \end{bmatrix}, \tag{1}$$

where $M_1(t)$, $M_2(t)$, and $M_3(t)$ are the Out-of-Plane (OoP) bending moments measured at the root of each blade; M_t and M_y are the tilt and yaw moments at the fixed frame, respectively; t is the time instant; ψ is the azimuth angle of the first blade; and $\mathbf{T}(\psi)$ is the direct MBC transformation matrix. The matrix $\mathbf{T}$ is defined as

$$\mathbf{T}(\psi) = \frac{2}{3} \begin{bmatrix} \cos(n\psi) & \cos\left(n\left(\psi + \frac{2\pi}{3}\right)\right) & \cos\left(n\left(\psi + \frac{4\pi}{3}\right)\right) \\ \sin(n\psi) & \sin\left(n\left(\psi + \frac{2\pi}{3}\right)\right) & \sin\left(n\left(\psi + \frac{4\pi}{3}\right)\right) \end{bmatrix}, \tag{2}$$

where n is the harmonic number ($n = 1$ for 1P loads).

Once the tilt and yaw moments have been obtained in the fixed frame, a control strategy is implemented to generate two pitch components. These components are used to reduce the 0P component of the aforementioned moments in the fixed frame, which correspond to the 1P component of the OoP moments in the rotational frame (Henry et al., 2023). The control strategy typically used is a decentralized control with integral (I) controllers. The control laws for these tilt and yaw components are given by:

$$\begin{cases} \beta_t = -k_t \int_0^t M_t dt \\ \beta_y = -k_y \int_0^t M_y dt \end{cases}, \tag{3}$$

where β_t and β_y are the pitch commands for the tilt and yaw moments, respectively, in the fixed frame, and k_t and k_y are the integral gains of the tilt and yaw controllers, respectively. The objective of these controllers is to bring the tilt and yaw moments to zero, thus reducing the cyclic loads on the blades.

After calculating the pitch commands in the fixed frame, the inverse MBC transformation is applied to map these commands back to the rotating frame, where they are applied as individual pitch commands for each blade. The inverse transformation is given by

$$\begin{bmatrix} \beta_{IPC1}(t) \\ \beta_{IPC2}(t) \\ \beta_{IPC3}(t) \end{bmatrix} = \mathbf{T}^{-1}(\psi) \begin{bmatrix} \beta_t(t) \\ \beta_y(t) \end{bmatrix}, \tag{4}$$

where $\beta_{IPC1}(t)$, $\beta_{IPC2}(t)$, and $\beta_{IPC3}(t)$ are the individual pitch commands for each blade and $\mathbf{T}^{-1}$ is the inverse MBC transformation matrix. The final pitch command for each blade is the sum of the collective CPC pitch command and the individual IPC command. An example of this formulation can be found in (Bossanyi, 2003).

Table 1
IEA 15 MW RTW properties.

Property	Value
Power rating	15 MW
Rotor orientation, configuration	Upwind, 3 blades
Cut-In, Rated Rotor Speed	5 rpm, 7.56 rpm
Cut-In, Rated, Cut-Out Wind Speed	3 m/s, 10.59 m/s, 25 m/s
Drivetrain	Low speed. Direct drive
Rated Generator Torque	19786767.5 Nm
Electrical Generator Efficiency	95.756 %
Rotor, Hub Diameter, Hub height	240 m, 7.94 m, 150 m
Rotor nacelle assembly mass	1070000 kg
Tower Mass	860000 kg
Blade pitch angle limits	0–90 deg
Pitch slew-rate limits	2 deg/s
Generator torque slew-rate limits	4500000 Nm/s

3. Proposed methodology

3.1. Environment for the modeling and simulation of wind turbines

This study focuses on the co-simulation of a wind turbine model using MATLAB/Simulink software, supported by OpenFAST software (Bonnie Jonkman, 2023). This approach allows a detailed simulation of the operating conditions of the wind turbine, facilitating analysis and

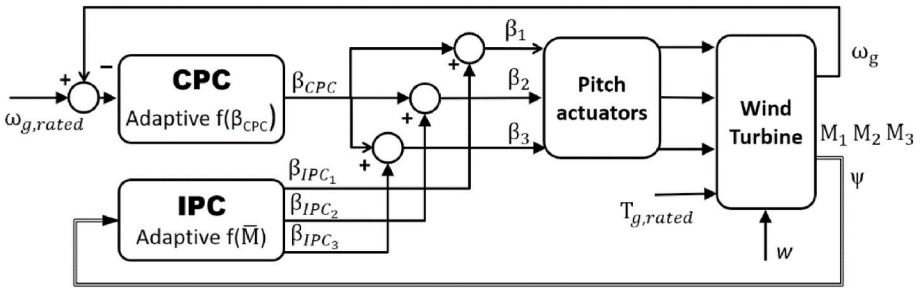

Fig. 2. IPC + CPC control system scheme for the full-load region. The CPC provides a common pitch command angle for the blades to regulate the generator rotational speed at its rated value. Meanwhile, the IPC determines a distinct action for each blade to reduce the blade moments.

improvement of the control strategies. In this particular case, the IEA 15 MW wind turbine reference model was used (Niranjan and Ramisetti, 2022). The turbine was configured as a monopile offshore turbine, and its main specifications are detailed in Table 1 (Gaertner et al., 2020). The key specifications of this wind turbine are as follows: it has a rated power output of 15 MW, a rated rotor speed of 7.56 rpm, and a rated wind speed of 10.59 m/s. In addition, the blade pitch actuator is subject to a rate of change limit of 2° per second. The turbine operates exclusively in the full load region, where the blades experience high stresses due to increasing bending moments as the average wind speed increases (Natarajan, 2022). In this specific region, a Proportional-Integral (PI) controller adjusts the blade pitch angle to regulate the rotor speed to its nominal value, while the torque controller saturates at the nominal torque.

Since the OpenFAST wind turbine model does not consider the dynamics of the pitch actuators, the pitch actuators are modeled by a second-order transfer function with unity gain, a damping factor of 0.707 and a natural frequency of 3.14 rad/s. The different proposed IPCs are adjusted by using an optimization process, whose objective is to minimize the average value of the DEL in the OoP moments of the blades.

TurbSim was used to generate the turbulent wind field required for the simulations (Jonkman, 2009). In particular, five operating points corresponding to the following average wind speeds were considered: 14, 16, 18, 20, and 22 m/s. The wind profiles were designed according to the IEC standard (I. IEC, 2005), using a Kaimal turbulence spectrum, with a hub turbulence intensity of 10 % and a vertical shear characterized by a power law exponent of 0.2. The sampling frequency for the simulations was 200 Hz. TurbSim ensures that the simulated wind conditions are representative of the real scenarios faced by wind turbines during operation, thus providing accurate data to evaluate the performance and response of the control system under different turbulence conditions. In this study, still water was assumed because waves are not a determining factor in the study of blade fatigue for monopile offshore wind turbines.

3.2. Proposed control scheme

The control scheme adopted in this research, depicted in Fig. 2, consists of the integration of two control loops: a CPC and an IPC. The individual pitch signals are added to the collective pitch signal to obtain the final required pitch angle for each blade. Since the wind turbine operates at rated power within the full load region, the generator torque, T_g, remains constant at its rated value.

For the CPC, a pre-designed PI controller with gain scheduling was used, which is based on the open-source reference controller ROSCO, in line with the parameters studied in (Abbas et al., 2022). The function of the CPC is to efficiently counteract wind speed variations and ensure that the generator speed ω_g is maintained at its rated value, while IPC is responsible for reducing the cyclic loads on the blades, which are associated with various harmonic components.

In IPC, the model of the process linearized at an operating point can be defined by the 2 × 2 transfer matrix **G**(*s*) in (5), where the controlled variables are the tilt and yaw moments, and the control signals are the tilt and yaw pitch signals. If a conventional decoupling network **D**(*s*) as shown in Fig. 1(a) is designed to achieve a diagonal apparent process **G**(*s*)**D**(*s*) equal to the diagonal elements of **G**(*s*), the decoupling network in (6) is required. This is called ideal decoupling (Garrido et al., 2011) and

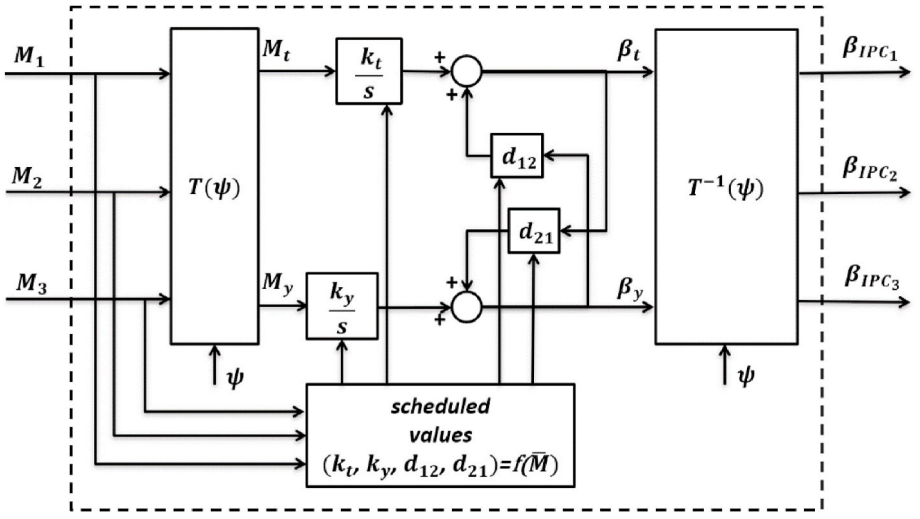

Fig. 3. General 1P IPC scheme with static inverted decoupling and a decentralized control composed of two integral controllers, the forward MBC transformation **T**(ψ) and the inverse MBC transformation.

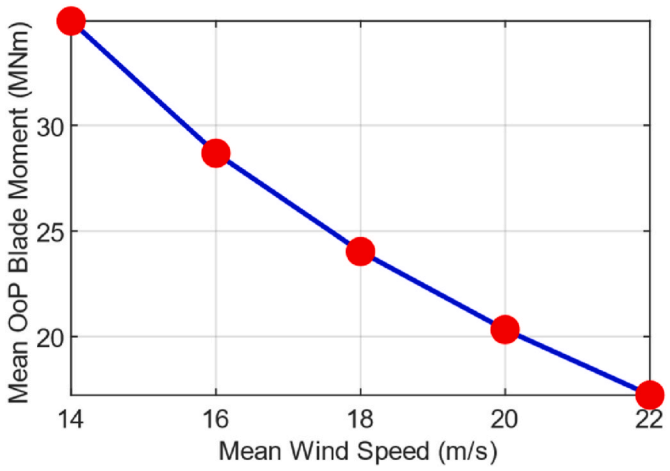

Fig. 4. Relationship between the mean OoP blade moment and the mean wind speed for the IEA 15 MW RWT operating in the nominal region.

its decoupling elements can be very difficult to implement. However, using the inverted decoupling structure of Fig. 1(b), this diagonal apparent process can be obtained with the two decoupling elements in (7), which are simpler to calculate and implement. These decupling elements do not directly correspond to the elements of a decoupling matrix $\mathbf{D}(s)$; however, inverted decoupling structure is an alternative approach for implementing conventional ideal decoupling. As shown in (Garrido et al., 2011), inverted decupling structure is equivalent to the conventional decoupling matrix in (8).

$$\begin{pmatrix} M_t(s) \\ M_y(s) \end{pmatrix} = \mathbf{G}(s) \begin{pmatrix} \beta_t(s) \\ \beta_y(s) \end{pmatrix} = \begin{pmatrix} g_{11}(s) & g_{12}(s) \\ g_{21}(s) & g_{22}(s) \end{pmatrix} \begin{pmatrix} \beta_t(s) \\ \beta_y(s) \end{pmatrix} \tag{5}$$

$$\mathbf{D}(s) = \mathbf{G}^{-1}(s) \begin{pmatrix} g_{11}(s) & 0 \\ 0 & g_{22}(s) \end{pmatrix} = \frac{\begin{pmatrix} g_{11}(s)g_{22}(s) & -g_{12}(s)g_{22}(s) \\ -g_{21}(s)g_{11}(s) & g_{11}(s)g_{22}(s) \end{pmatrix}}{g_{11}(s)g_{22}(s) - g_{12}(s)g_{21}(s)} \tag{6}$$

$$d_{12}(s) = \frac{-g_{12}(s)}{g_{11}(s)} \text{ and } d_{21}(s) = \frac{-g_{21}(s)}{g_{22}(s)} \tag{7}$$

$$\mathbf{D}(s) = \frac{\begin{pmatrix} 1 & d_{12}(s) \\ d_{21}(s) & 1 \end{pmatrix}}{1 - d_{12}(s)d_{21}(s)} \tag{8}$$

When focusing on low frequency interactions, the decoupling elements can be calculated on the basis of the steady-state gains matrix $\mathbf{G}(0)$ and using the expressions in (7) with $s = 0$. This static inverted decoupling makes the apparent process (the combination of the process and the decoupling network) diagonal in steady state with the diagonal elements of $\mathbf{G}(0)$ ($g_{11}(0)$ and $g_{22}(0)$). These two steady-state gains can be used to reduce undesired interactions at low frequencies between the two controlled variables, improving the performance of the IPC system.

As shown in Fig. 3, the IPC scheme implemented in this research incorporates the MBC transform for the 1P harmonic, the internal control to reduce the M_t and M_y moments, and the inverse MBC transform. The internal control scheme consists of two integral controllers and, in addition, the possibility of including two decoupling gains (d_{12} and d_{21}) following the structure of the inverted decoupling previously described.

Variations in wind speed, w, modify the operating point of the wind turbine and consequently affect the performance of the control system. In this paper, an adaptive control by gain-scheduling was proposed to ensure that the control system performed properly under different wind conditions. To create an adaptive IPC, the controller was tuned for five operating points according to the wind conditions. However, the wind speed was not used as a scheduling variable; instead, it was proposed to use the mean value $\overline{M}$ of the filtered blade moments (Lara et al., 2023).

Other studies have used the mean wind speed as the adjustment variable (Serrano et al., 2022); however, this approach requires additional sensors or estimators. In contrast, the proposed scheduling variable, the mean momentum $\overline{M}$, can be easily calculated from the blade moment measurements already employed in the IPC, which simplifies the implementation of the adaptive control system. We assumed a monotonic relation between the operation point and the load since only the above-rated region is considered. In this region, the average moment $\overline{M}$ depends almost entirely on the average wind speed, and the higher the wind speed, the lower the average blade moment. Fig. 4 shows this relationship for the five operating points considered for the IEA 15 MW wind turbine. Although the average moment decreases with wind speed, the periodic components of these moments, the amplitude of their fluctuations, and their standard deviation increase with wind speed and turbulence. It is for this reason that the DEL value of the OoP bending moments of the blades also increases, and this is what the IPC seeks to reduce.

Once the optimal parameters are obtained for each operating point, the adaptive gain-scheduled IPC calculates the required control parameters by linear interpolation of the optimal parameters based on the mean value $\overline{M}$ of the filtered blade moments. This allows the control to continuously adjust to variations in the operating conditions.

3.3. Individual pitch controllers under study

We designed and compared different IPCs, classified according to the number and type of parameters (degrees of freedom) to be adjusted and how these are calculated. The parameters k_t and k_y represent the integral tilt and yaw gains, respectively. In addition, the IPC schemes include two additional gains due to the static inverted decoupling (d_{12} and d_{21}). Depending on the case, the integral gains can be forced to be equal or not, the decoupling elements can also be forced to be equal in absolute value or not, and they can be calculated based on prior knowledge of the process or by optimization. The integral gains are calculated by optimization except for one case, IPC2, where they are retuned based on IPC1 and the decoupling elements. Combining these factors, eight IPCs are proposed for a comprehensive comparison of IPC configurations, evaluating their performance in terms of blade load reduction. The proposed IPCs are as follows.

- IPC1 (I1): two identical integral controllers are used, as they are required to have the same gain; no decoupling is used. Therefore, $k_t = k_y$ and $d_{12} = d_{21} = 0$. The common controller gain is only parameter to tune. This is considered as the baseline control that is intended to be improved by the inclusion of static inverted decoupling.
- IPC2 (ID): two decoupling elements are used, calculated based on prior knowledge of the steady state dynamics of the system, that is, the steady-state gain matrix $\mathbf{G}(0)$. Then the integral gains of IPC1 are retuned by multiplying by a correction factor proposed in (Hägglund et al., 2022) and equal to $(1\text{-}d_{12}d_{21})$. This factor corresponds to the denominator in (8) and it removes the change of gain in the controllers produced by the static decoupling network. No optimization is performed.
- IPC3 (I1D): two equal integral controllers ($k_t = k_y$) and two decoupling elements are used, the latter being calculated before optimization in the same way as in IPC2. There is one parameter to optimize: the common integral controller gain.
- IPC4 (I2D): is similar to IPC 3 but two different integral controllers ($k_t \neq k_y$) are used. The decoupling elements are calculated before optimization in the same way as in IPC2 and IPC3. There are two parameters to optimize: the two different integral gains of the controllers.
- IPC5 (I1D1): two identical integral controllers are used ($k_t = k_y$), and two decoupling elements identical in absolute value, but of opposite

Table 2
Steady-state gains of the process and static decoupling elements for different operating points.

w (m/s)	$g_{11}(0)$ (kNm/rad)	$g_{12}(0)$ (kNm/rad)	$g_{21}(0)$ (kNm/rad)	$g_{22}(0)$ (kNm/rad)	d_{12}	d_{21}
14	$-1.8926{\cdot}10^5$	$2.0605{\cdot}10^5$	$-2.0689{\cdot}10^5$	$-1.9061{\cdot}10^5$	1.09	−1.09
16	$-1.9723{\cdot}10^5$	$2.1765{\cdot}10^5$	$-2.1923{\cdot}10^5$	$-1.9867{\cdot}10^5$	1.10	−1.10
18	$-1.9929{\cdot}10^5$	$2.2746{\cdot}10^5$	$-2.3224{\cdot}10^5$	$-2.0356{\cdot}10^5$	1.14	−1.14
20	$-1.9498{\cdot}10^5$	$2.3787{\cdot}10^5$	$-2.4872{\cdot}10^5$	$-2.0763{\cdot}10^5$	1.21	−1.21
22	$-1.8453{\cdot}10^5$	$2.4708{\cdot}10^5$	$-2.6761{\cdot}10^5$	$-2.0578{\cdot}10^5$	1.34	−1.34

sign (d_{12} = -d_{21}). The reason behind this choice is discussed later. There are two parameters to be optimized: the common integral gain of the controllers and the common absolute value of the decoupling elements.

- IPC6 (I1D2): an identical integral gain ($k_t = k_y$) and two different decoupling elements are used. There are three parameters to optimize: the common integral controller gain and the two decoupling elements.
- IPC7 (I2D1): two different integral controllers ($k_t \neq k_y$) and two decoupling elements identical in absolute value but of opposite sign ($d_{12} = -d_{21}$) are used. There are three parameters to optimize: the two controller gains and the common absolute value of the decoupling element.
- IPC8 (I2D2): two different integral controllers ($k_t \neq k_y$) and two different decoupling elements are used. There are four parameters to optimize: the two controller gains and the two decoupling elements.

3.4. Calculation of the stationary inverted decoupling elements

One of the central objectives of this study is to address the IPC control problem related to the coupling present in the two control loops of the moments on the non-rotational axes within the MBC transformation. In this context, the process is treated as a multivariable system with two output variables (the moments M_t and M_y) controlled by two manipulated variables (the pitch signals β_t and β_y).

In the proposed IPCs 2, 3, and 4 (ID, I1D, and I2D), the static decoupling elements are calculated not by optimization but on the basis of the steady-state gains of such a linearized 2 × 2 process at an operating point. This steady-state process at an operating point is defined by (5) doing $s = 0$ and the decoupler gains d_{12} and d_{21} are calculated using (7) with $s = 0$.

The non-linearity of the system generates variations in the approximate linear models, depending on the operating point. Table 2 shows the steady-state gains of the 2 × 2 process for the IPC in the operating points considered, as well as the corresponding decoupling elements calculated according to (7). The decoupling elements present practically equal values (although of opposite sign) without significant differences in the absolute value, so they are set to an equal and intermediate value for each operating point. This is the reason why we propose using two decoupling elements identical in absolute value but of opposite sign (d_{12} = -d_{21}) in some of the studied IPCs.

3.5. IPC tuning by optimization via genetic algorithms

The tuning of the IPC parameters is carried out through an optimization process, the main objective of which is to minimize the fatigue load on the blades, taking into account the OoP moments of the blades. For the fatigue assessment of wind turbines, the DEL index is usually calculated offline from the time series of the simulation data using cycle counting techniques. This implies that the assessment of the DEL cannot be performed analytically in real time. To facilitate this process, the MLife script suite of NREL (MLife wind research) was used for the post-processing of the data generated in each simulation, allowing the corresponding DEL values to be extracted.

In the framework of the proposed optimization, the mean DEL value of the three OoP moments of the blades, denoted as DEL(M), is the objective function to be minimized, i.e., the cost function J. Afterwards, the designs are assessed by multiple simulations with winds generated with same turbulent properties but different turbulent seeds. The formulation of the optimization problem is expressed as follows:

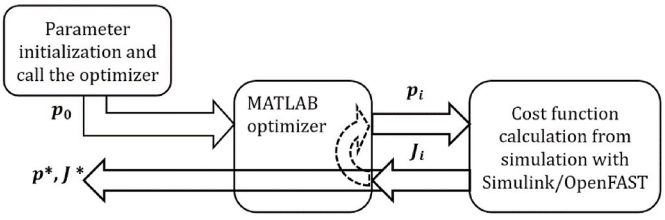

Fig. 5. Simulation-based optimization process.

$$\begin{aligned} &min\ DEL(M) = \sum_{i=1}^{3} DEL(M_i(p)) \Big/ 3 \\ &\quad subject\ to \\ &\quad \text{solution of the} \\ &\quad \text{model} \\ &\quad p \in S \end{aligned} \tag{9}$$

The IPC tuning parameters determine the vector p of the decision variables. According to the IPC scheme, the dimensionality of the parameter vector varies from one to four. Consequently, the solution space S is constrained as follows.

- $S \in \mathbb{R}^1$ for IPC1 and IPC3 in which only an integral gain is optimized, where $k_t = k_y$ and decoupling elements are zero (IPC1) or they are calculated and fixed beforehand (IPC3). These cases represent the simplest configurations for optimization.
- $S \in \mathbb{R}^2$ for IPC4, which considers two different integral gains, and the decoupling elements are pre-calculated, and for IPC5, which sets identical integral gains and decoupling elements equal in absolute value.
- $S \in \mathbb{R}^3$ for IPC6 (I1D2), which provides for two equal integral gains and different decoupling elements, and for IPC7 (I2D1), which provides for different integral gains and an equal absolute value of the decoupling element.
- $S \in \mathbb{R}^4$ for IPC8 involving two different integral gains and two different decoupling elements. This is the most complex case for optimization.

The main objective of the optimization is to reduce the DEL of the blades, which is influenced by the parameter vector p. This process considers the dynamic behavior of the wind turbine model and the control system and is subject to the constraints defined in the solution space S. Given that the cost function J and the dynamic model of the wind turbine in OpenFAST are highly complex and cannot be evaluated analytically, the proposed optimization is carried out using a simulation-based approach, as illustrated in Fig. 5. First, the initial values of the decision variables are set in the vector p_0. Then, the optimization

Table 3
Optimization results for different IPCs at the five operation points.

IPC scheme	Parameter	Wind speed (m/s)				
		14	16	18	20	22
1 I1	DEL(M) (MNm)	17.00	16.27	18.74	22.32	16.73
	$k_t = k_y$ (rad/kNms)	$5.20{\cdot}10^{-7}$	$4.35{\cdot}10^{-7}$	$1.63{\cdot}10^{-7}$	$1.34{\cdot}10^{-7}$	$8.47{\cdot}10^{-8}$
2 ID	DEL(M) (MNm)	15.68	15.07	18.36	20.37	15.54
	$k_t = k_y$ (rad/kNms)	$1.14{\cdot}10^{-6}$	$9.61{\cdot}10^{-7}$	$3.75{\cdot}10^{-7}$	$3.30{\cdot}10^{-7}$	$2.32{\cdot}10^{-7}$
	$d_{12} = -d_{21}$	1.09	1.10	1.14	1.21	1.32
3 I1D	DEL(M) (MNm)	15.24	15.01	16.50	17.89	13.90
	$k_t = k_y$ (rad/kNms)	$1.73{\cdot}10^{-6}$	$2.46{\cdot}10^{-6}$	$2.96{\cdot}10^{-6}$	$3.08{\cdot}10^{-6}$	$3.75{\cdot}10^{-6}$
	$d_{12} = -d_{21}$	1.09	1.10	1.14	1.21	1.32
4 I2D	DEL(M) (MNm)	14.99	14. 97	16.34	17.65	13.89
	k_t (rad/kNms)	$1.63{\cdot}10^{-6}$	$2.54{\cdot}10^{-6}$	$2.83{\cdot}10^{-6}$	$1.86{\cdot}10^{-6}$	$3.48{\cdot}10^{-6}$
	k_y (rad/kNms)	$1.07{\cdot}10^{-6}$	$1.43{\cdot}10^{-6}$	$4.72{\cdot}10^{-6}$	$3.86{\cdot}10^{-6}$	$3.76{\cdot}10^{-6}$
	$d_{12} = -d_{21}$	1.09	1.10	1.14	1.21	1.32
5 I1D1	DEL(M) (MNm)	14.39	14. 68	16.23	17.23	13.40
	$k_t = k_y$ (rad/kNms)	$5.27{\cdot}10^{-6}$	$5.39{\cdot}10^{-6}$	$7.20{\cdot}10^{-6}$	$8.30{\cdot}10^{-6}$	$7.99{\cdot}10^{-6}$
	$d_{12} = -d_{21}$	4.83	3.03	1.98	5.00	3.73
6 I1D2	DEL(M) (MNm)	14.35	14. 67	16.13	17.21	13.39
	$k_t = k_y$ (rad/kNms)	$1.61{\cdot}10^{-5}$	$6.50{\cdot}10^{-6}$	$6.56{\cdot}10^{-6}$	$5.33{\cdot}10^{-6}$	$7.56{\cdot}10^{-6}$
	d_{12}	5.52	3.79	1.58	6.50	3.61
	d_{21}	−6.40	−2.13	−2.32	−2.83	−3.73
7 I2D1	DEL(M) (MNm)	14.35	14. 67	16.18	17.23	13.39
	k_t (rad/kNms)	$1.27{\cdot}10^{-5}$	$6.21{\cdot}10^{-6}$	$5.11{\cdot}10^{-6}$	$6.87{\cdot}10^{-6}$	$9.70{\cdot}10^{-6}$
	k_y (rad/kNms)	$1.62{\cdot}10^{-5}$	$4.62{\cdot}10^{-6}$	$6.75{\cdot}10^{-6}$	$7.74{\cdot}10^{-6}$	$8.06{\cdot}10^{-6}$
	$d_{12} = -d_{21}$	5.23	3.06	1.71	4.59	4.10
8 I2D2	DEL(M) (MNm)	14.33	14. 64	16.11	17.20	13.38
	k_t (rad/kNms)	$6.69{\cdot}10^{-6}$	$4.80{\cdot}10^{-6}$	$5.39{\cdot}10^{-6}$	$6.42{\cdot}10^{-6}$	$7.88{\cdot}10^{-6}$
	k_y (rad/kNms)	$3.39{\cdot}10^{-6}$	$3.83{\cdot}10^{-6}$	$6.16{\cdot}10^{-6}$	$8.27{\cdot}10^{-6}$	$7.96{\cdot}10^{-6}$
	d_{12}	6.69	4.74	2.53	3.47	3.51
	d_{21}	−3.14	−4.03	−1.52	−4.89	−3.84

procedure initiates an iterative loop. In each iteration of this loop, the optimizer in MATLAB performs various co-simulations using OpenFAST/Simulink, calculates the objective function J, and searches for the optimal solution p^*. This process results in a nonlinear problem that requires a considerable number of calculations and computational time.

The different IPC schemes are optimized by simulating the IEA 15 MW wind turbine model at the five operating points defined earlier. Each simulation lasts for 800 s, with the first 200 s discarded to eliminate transient effects. This ensures that the collected data reflect the stable behavior of the turbine during operation. During each iteration of the procedure, the effects of different parameter configurations on the turbine performance are evaluated. At the end of each cycle, the optimizer adjusts the parameter values based on the results obtained, effectively seeking the configuration that reduces DEL(M) throughout the simulations.

The proposed optimization process represents a complex nonlinear problem that requires considerable computational effort. To improve the efficiency of the calculations, the optimizer uses a genetic algorithm. Genetic algorithms are optimization and search techniques inspired by the natural selection process in biology. These algorithms use mechanisms such as mutation, crossover and selection to generate increasingly better solutions to a given problem. They work with a population of possible solutions that evolve iteratively, selecting the best ones and combining them to create new generations of solutions. This technique is particularly suitable for complex problems because it effectively explores the solution space, finding parameters that minimize the cost function J quicklier than traditional methods. The basic concepts (selection, crossover, mutation, elitism) and theoretical foundations of the implemented algorithm are detailed in (Goldberg, 1989), (Goldberg and Deb, 1991). In the proposed optimization, the chromosomes are composed of the parameters (k_t, k_y) for the IPC controllers without inverted decoupling and (k_t, k_y, d_{12}, d_{21}) for the IPC controllers that include inverted decoupling. The search ranges for the integral gains are set between [0–$5{\cdot}10^{-5}$] rad·kNm^{-1}s^{-1}, while the elements of the inverted decoupling are restricted to the interval [0–10] in absolute value. The population is configured with 625 individuals ($5 \times 5 \times 5 \times 5$) for IPC that requires tuning of four parameters; for those requiring one or two parameters, the population size is 100, and for IPCs with three parameters, it is set to 250. An elite count equivalent to 5 % of the population size was used for reproduction, a crossover fraction of 0.8, and a mutation probability of 0.2 for generating offspring. In this study, the optimization process is stopped after reaching 50 generations without changes in the best fitness, as this number has been observed to be sufficient for achieving convergence in the proposed optimization.

4. Results and discussion

4.1. Optimization results

This section presents the results obtained after the optimization of the IPC schemes at five operating points in the full-load region for wind speeds ranging from 14 to 22 m/s. Table 3 shows the DEL(M) values, the

Table 4
Relative DEL(M) values of the proposed IPCs with respect to the baseline IPC1.

Wind Speed (m/s)	2 ID	3 I1D	4 I2D	5 I1D1	6 I1D2	7 I2D1	8 I2D2
14	92.24 %	89.65 %	88.18 %	84.65 %	84.41 %	84.41 %	84.29 %
16	92.63 %	92.26 %	92.01 %	90.23 %	90.17 %	90.17 %	89.98 %
18	98.01 %	88.05 %	87.19 %	86.61 %	86.07 %	86.34 %	85.97 %
20	91.29 %	80.15 %	79.08 %	77.20 %	77.11 %	77.20 %	77.06 %
22	92.88 %	83.08 %	83.02 %	80.10 %	80.04 %	80.04 %	79.98 %

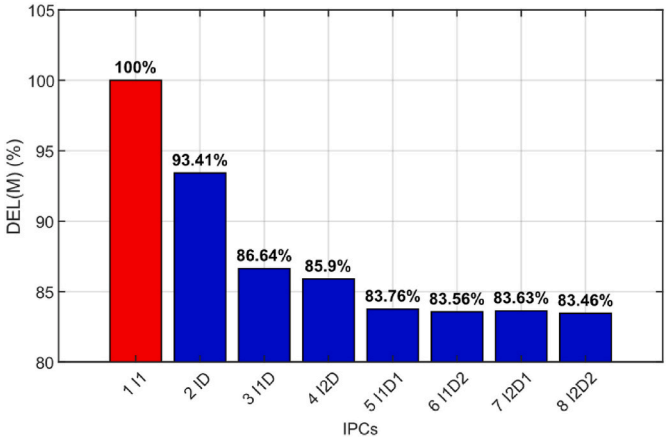

Fig. 6. Relative DEL(M) values for the proposed IPCs with respect to the baseline IPC1.

integral gains k_t and k_y, and the decoupling elements d_{12} and d_{21} for each proposed control scheme. To evaluate the effectiveness of the strategies, the IPC1 (I1) scheme, which corresponds to the controller with a single adjustable parameter and no decoupling, was taken as the baseline. Table 4 shows the relative values of the DEL(M) for each control scheme with respect to the IPC 1 (baseline) at each wind speed. Fig. 6 shows a bar chart with the average values of relative DEL(M) of the five operating points analyzed for each control scheme with respect to the baseline IPC1.

From the comparison of the different control schemes at each operating point with respect to the baseline IPC1, the following can be stated.

- The incorporation of static inverted decoupling improves the baseline IPC1 control in all cases in the reduction of the DEL(M). A reduction between 6 % and 16 % is achieved depending on the IPC considered.
- The IPC2 (ID), which only needs to manually determine the decoupling elements and readjust the integral gains of the baseline IPC, manages to reduce the DEL(M) by more than 7 % except around 18 m/s, where this reduction is only about 2 %. This scheme only requires calculating the decoupling elements based on the stationary-state gain matrix of the process in (5) according to (6) and readjusting the integral gains by multiplying by a simple computation factor. These parameters vary slightly depending on the wind speed.
- The IPC3 (I1D) introduces the previous manually calculated decoupling elements and optimizes the integral gains, which are forced to be equal ($k_t = k_y$). It reduces the DEL(M) by a mean of 13.36 %, particularly standing out at 20 m/s, where it achieves a reduction of 19.85 %. This is a significant improvement over the baseline control, maintaining the design simplicity without increasing the computational complexity.
- The IPC4 (I2D) uses the same decoupling elements as the previous IPCs and optimizes the two integral gains, allowing them to be different. Although it introduces an additional parameter to optimize, it does not significantly improve the previous IPC2, achieving a DEL(M) reduction of only 14.10 %, with maximum reductions of 21 % at wind speeds between 20 and 22 m/s.
- The IPC5 (I1D1) forces equal integral gains and decoupling elements of equal absolute value and optimizes both parameters. This allows for greater adaptability to wind conditions, achieving a DEL(M) reduction of 16.25 %, with a maximum of 22.80 % at 20 m/s. This scheme represents a remarkable balance between simplicity and effectiveness, as it adds only one additional parameter to optimize and improves performance by nearly 3 % more than IPC3 (I1D).
- The IPC6 (I1D2) optimizes two decoupling elements and an integral gain ($k_t = k_y$). This scheme achieves a DEL(M) reduction of 16.44 %, with a maximum of 22.89 % at 20 m/s. Despite its additional complexity with three parameters to optimize, it provides almost no improvement over the previous control, IPC5, which offers similar improvements with one less parameter.
- The IPC7 (I2D1) also optimizes the three parameters and achieves similar DEL reductions as the previous controls IPC5 and IPC6.
- IPC8 (I2D2), despite optimizing four parameters, achieves similar DEL reduction as the previous three IPCs, but only slightly higher.

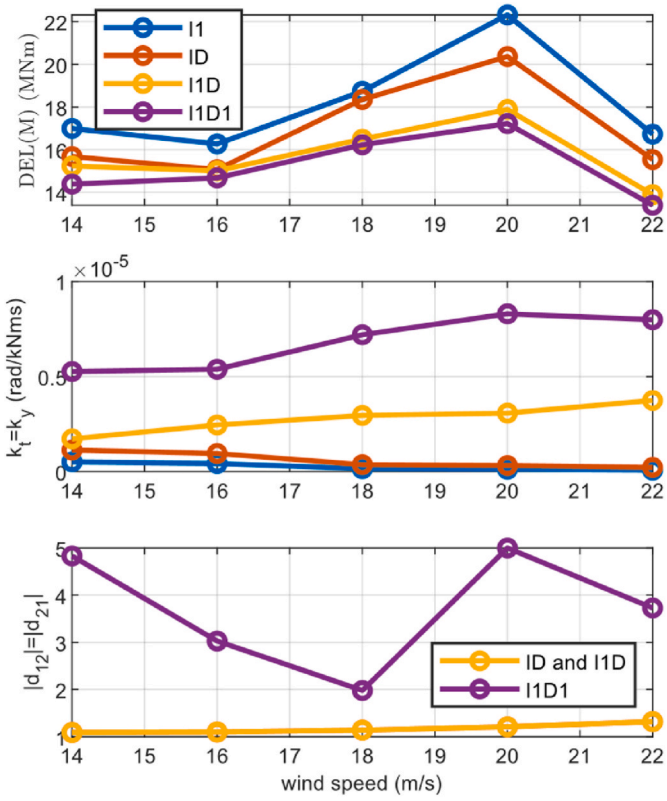

Fig. 7. Graphical representation of the optimization results of the controller gains k_t and k_y, the common decoupling gains, and the mean DEL value of the OoP blade moments with respect to the five wind speeds considered in the nominal region for the IPCs 1, 2, 3, and 5.

Following the above analysis, the IPC2 (ID) stands out for its

Table 5
Average performance indicators for the IPCs calculated from the simulation data for each simulation case.

IPC scheme	$\overline{\text{DEL}}$ (M) (MNm)			$\overline{\text{NAT}}$ (β) (%)		
	Case 1	Case 2	Case 3	Case 1	Case 2	Case 3
1 I1	20.26 (100.00 %)	21.46 (100.00 %)	22.23 (100.00 %)	42.9 (100.00 %)	43.69 (100.00 %)	47.05 (100.00 %)
2 ID	18.08 (89.25 %)	18.95 (88.30 %)	20.75 (93.35 %)	39.53 (92.15 %)	41.94 (96.00 %)	46.64 (99.13 %)
3 I1D	17.53 (86.53 %)	17.70 (82.46 %)	19.58 (88.07 %)	41.19 (96.10 %)	44.25 (101.20%)	50.78 (107.83 %)
4 I2D	17.57 (86.71 %)	17.73 (82.60 %)	19.11 (85.95 %)	41.06 (95.83 %)	44.40 (101.51 %)	50.23 (106.63 %)
5 I1D1	17.26 (85.17 %)	17.77 (82.82 %)	19.19 (86.31 %)	41.01 (95.65 %)	44.46 (101.64 %)	49.74 (105.58 %)
6 I1D2	17.29 (85.34 %)	17.70 (82.46 %)	19.28 (86.75 %)	41.35 (96.54 %)	44.45 (101.56 %)	49.64 (105.34 %)
7 I2D1	17.24 (85.10 %)	17.67 (82.34 %)	19.15 (86.13 %)	41.07 (95.83 %)	44.32 (101.35 %)	49.64 (105.38 %)
8 I2D2	17.52 (86.49 %)	17.68 (82.40 %)	19.13 (86.06 %)	40.59 (94.66 %)	44.07 (100.77 %)	49.70 (105.50 %)

simplicity of calculation from a previous IPC design, without the need for optimization, although it achieves only about half the DEL reduction of the other proposed IPCs. The IPC3 (I1D) stands out for its simplicity and effectiveness. With only one parameter to optimize, it achieves almost twice the DEL(M) reduction of IPC2 with values close to the other IPCs. The IPC5, with only two parameters to optimize, achieves a DEL (M) reduction of 16.25 %, almost 3 % more than IPC2. These two cases (IPC3 and IPC5) are the most effective in terms of DEL reduction and calculation simplicity. The other IPCs with more parameters to optimize are not justified by the small improvement in DEL reduction. Therefore, these three IPCs will be studied in more detail in comparison with the baseline IPC1.

A graphical representation of the data from these selected schemes is shown in Fig. 7, where the integral gains of the IPC, the decoupling elements, and the DEL(M) values are presented as a function of the wind speed. From Fig. 7, we can analyze the variations of the control parameters (k_t, k_y, d_{12}, and d_{21}) in the selected IPCs for different wind speeds. In the baseline control, the integral gains decrease with wind speed from $5.20{\cdot}10^{-7}$ rad/kNms at 14 m/s to $8.47{\cdot}10^{-8}$ rad/kNms at 22 m/s. This makes sense since the steady-state gains of the diagonal process controlled by the IPC tend to increase with wind speed (Table 2). However, by introducing static inverted decoupling in IPCs 2, 3, and 5, the integral gains are larger; furthermore, in IPCs 3 and 5, instead of decreasing with wind speed, the integral gains tend to increase. For example, in IPC3, the integral gains increase from $1.73{\cdot}10^{-6}$ rad/kNms to $3.75{\cdot}10^{-6}$ rad/kNms; and in IPC5, they increase from $5.27{\cdot}10^{-6}$ rad/kNms to $7.99{\cdot}10^{-6}$ rad/kNms. The optimization allows for greater sensitivity and responsiveness across the speed range adapted to the increase in dynamic loads with wind speed.

As for the decoupling elements, those calculated manually vary proportionally with wind speed increasing slightly in absolute value from 1.09 to 1.32. When this value is optimized (IPC5), the absolute values of the decoupling elements are significantly larger and vary nonlinearly between a peak of 5 and a minimum of 2.

4.2. Simulation results

This section evaluates in more detail the performance of the previously designed and implemented adaptive IPC schemes under more realistic conditions. For this purpose, three simulation cases were carried out using different wind profiles that included a stochastic turbulence component. The mean wind speed was kept within the nominal region in each case. These wind conditions were analyzed to study both the performance and robustness of the proposed adaptive IPC schemes.

The wind profiles were generated with the TurbSim tool, following the specifications of IEC 61400-1. Each simulation had a total duration of 1200 s, although the first 200 s were discarded to eliminate transient effects. In case 1, the mean wind speed ranged between 14 and 18 m/s; in case 2, between 16 and 20 m/s; and in case 3, between 18 and 22 m/s. For each case, six different simulations were performed using wind profiles with the same turbulent properties but different turbulent seeds. From the data obtained, the most relevant variables were analyzed in both the time and frequency domains for each control strategy. In addition, several performance indicators related to the blade moments and pitch actuator effort were calculated. In the analysis, the IPC1 (I1) was used as the baseline.

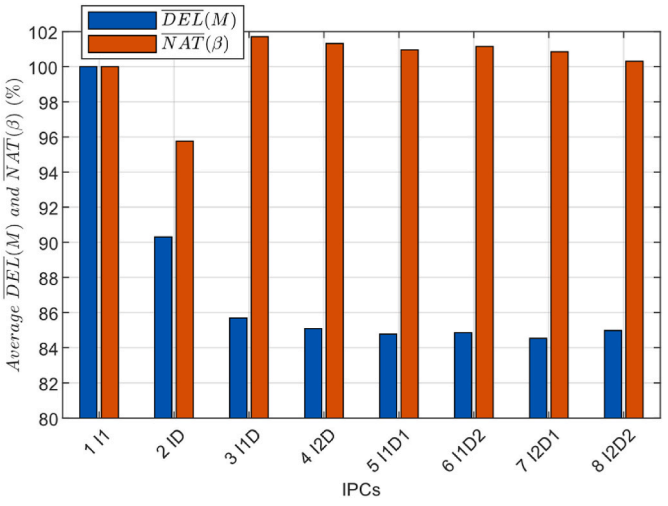

Fig. 8. Average values of the relative $\overline{\text{DEL}}$ (M) and $\overline{NAT}$ (β) values for the proposed IPCs with respect to the baseline IPC1.

Table 5 shows the average DEL(M) of the blades, denoted by $\overline{\text{DEL}}$ (M), over the six simulations with different seeds for the different proposed IPCs. The mean NAT of the three pitch actuators, NAT(β), was used to measure the control effort and is defined in (10) (Gambier, 2022). Table 5 also shows the average NAT(β), denoted by $\overline{\text{NAT}}$ (β). The DEL(M) and NAT(β) were calculated for each proposed IPC from data obtained from a 1000 s simulation and then averaged over the 6 different seed simulations. This allowed a comprehensive evaluation of the performance of each control scheme under different wind conditions. Fig. 8 shows a bar chart with the average relative $\overline{\text{DEL}}$ (M) and relative $\overline{\text{NAT}}$ (β) values of the proposed IPCs with respect to the baseline IPC1 averaged over the three simulation cases analyzed.

$$NAT(\beta) = \frac{1}{3}\sum_{i=1}^{3}\left(\frac{1}{T}\int_0^T \left|\frac{\dot{\beta}_i(t)}{\dot{\beta}_{\max}}\right| dt\right) \tag{10}$$

From Table 5 and Fig. 8, it can be stated that the static inverted decoupling manages to reduce the average DEL of the OoP moments of the blades with a control effort, given by the average $\overline{\text{NAT}}$ (β), similar to or even lower than the baseline IPC. As for the $\overline{\text{DEL}}$ (M), the proposed IPCs reduced it between 85.10 and 89.25 % in simulation case 1 with a $\overline{\text{NAT}}$ (β) of 92.15 % for IPC2 and values between 94.66 and 96.54 % for the rest of the IPCs. In case 2, the best performances were achieved with reductions of $\overline{\text{DEL}}$ (M) to values of 88.3 % for IPC2, and to values between 82.34 and 82.82 % for IPCs from 3 to 8. The $\overline{\text{NAT}}$ (β) of IPC2 was reduced to a value of 96 % while it is slightly increased to values

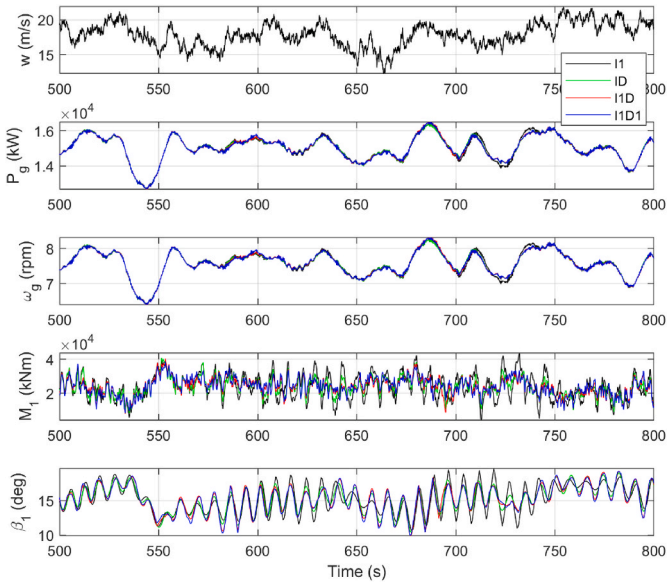

Fig. 9. Time responses in the rotating reference frame of wind speed (w), generator angular velocity (ω_g), generated power (P_g), OoP moment of blade 1 (M_1), and pitch signal of blade 1 (β_1).

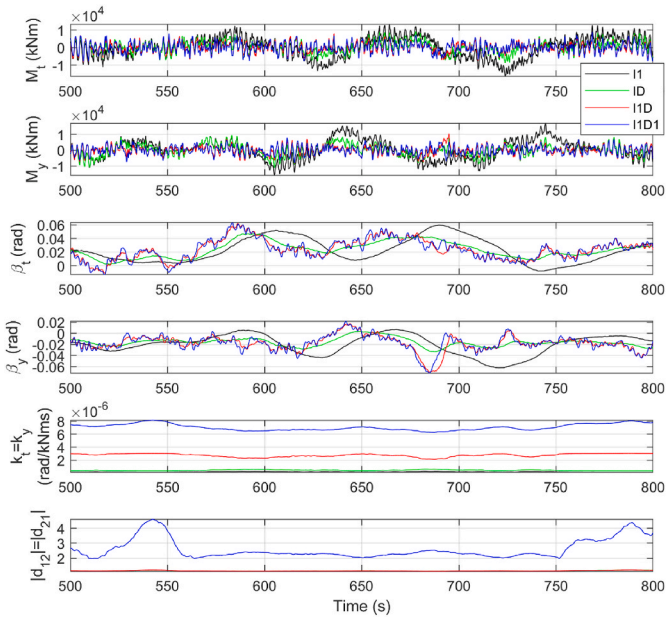

Fig. 10. Time responses of the IPC variables in the non-rotating reference frame: tilt moment (M_t), yaw moment (M_y), tilt pitch signal (β_t), yaw pitch signal (β_y), controller adaptive gains (k_t and k_y), and adaptive decoupling gain (d_{12}).

between 100.77 and 101.64 % for the remaining IPCs. Case 3 is the one with the worst values: IPC2 reduces the $\overline{DEL}$ (M) to only 93.35 %, while the other IPCs reduced it to values between 85.95 and 88.07 %; moreover, IPCs from 3 to 8 increased their $\overline{NAT}$ (β) between 5.34 and 7.83 % and IPC2 reduced it to 99.13 %.

In summary, IPC2 (ID) reduces $\overline{DEL}$ (M) the least, to only 90.30 % on average but is the IPC with the lowest average $\overline{NAT}$ (β) of 95.76 %. The remaining IPCs (from 3 to 8) achieve further average reductions of the $\overline{DEL}$ (M) to values between 84.53 % (for IPC7) and 85.69 % (for IPC3), while the average $\overline{NAT}$ (β), at around 101 % in almost all these cases, is very similar to that of IPC1; the somewhat slightly smaller noticeable increase in control effort is for IPC8, which has an average $\overline{NAT}$ (β) of 100.31 %. Considering the above analysis and the computational complexity of each proposed IPC, IPCs with more than two parameters to be optimized are not justified as they do not provide a noticeable improvement. The schemes that achieve a better compromise are IPC3 (I1D), IPC4 (I2D), and IPC5 (I1D1), with average reductions of the $\overline{DEL}$ (M) to 85.69, 84.77 and 85.09 %, and average $\overline{NAT}$ (β) values of 101.71 %, 101.32 and 100.96 %, respectively. The IPC2 (ID) also stands out, since although it presents a worse performance than the previous two in terms of DEL (90.30 %), it has a much higher computational facility and lower pitch actuator effort with an average $\overline{NAT}$ (β) of 95.76 %.

4.2.1. Time responses

Fig. 9 shows the time responses of some proposed IPC schemes compared to the baseline scheme IPC1, corresponding to simulation case 2. For ease of interpretation, only three highlighted IPCs are included: IPC2 (ID), IPC3 (I1D), and IPC5 (I1D1). In addition, to improve visualization, only 300 s of the simulations are presented. Fig. 9 shows specifically the wind speed w, the generated power P_g, the generator angular velocity ω_g, the OoP moment of blade 1 M_1, and the pitch signal of actuator 1 β_1. There were no significant differences in either the generated power or the generator speed. This shows that the improvement in the IPC schemes in terms of blade DEL reduction does not influence the CPC loop behavior. The standard deviation (STD) values of P_g and ω_g are practically identical for all IPCs in each of the cases analyzed: 496 kW and 0.25 rpm for case 1, 617 kW and 0.31 rpm for case 2, and 770 kW and 0.39 rpm for case 3.

In contrast, significant differences were observed in the variables associated with the IPC loop. The baseline IPC1 presented the largest oscillations in the OoP moments of the blades, while the other IPCs managed to considerably mitigate the amplitude of these oscillations. Similar responses were obtained in the other simulation cases. Table 6 and Fig. 10 present the results of the internal variables of the IPC in the non-rotational reference system corresponding to the simulations described previously. Table 6 shows the mean values and standard deviations of the tilt- and yaw-moments (M_t and M_y) obtained using the MBC transformation for each IPC under the three simulation cases. Fig. 10 shows the time response of these variables for simulation case 2, specifically the moments M_t and M_y, the tilt and yaw pitch signals (β_t and β_y), the evolution of the adaptive gains k_t and k_y of the controllers, and

Table 6
The mean and STD values of the non-rotating moments Mt and My calculated from the simulation data for each simulation case.

IPC scheme	$\overline{M_t}$ (MNm)			STD(M_t) (MNm)			$\overline{M_y}$ (MNm)			STD(M_y) (MNm)		
	Case 1	Case 2	Case 3	Case 1	Case 2	Case 3	Case 1	Case 2	Case 3	Case 1	Case 2	Case 3
1 I1	0.02	0.05	0.06	3.42	4.03	4.46	−0.02	0.03	0.018	3.42	4.07	4.41
2 ID	0.01	0.00	0.01	2.85	3.29	3.81	0.01	0.02	0.02	2.68	3.22	3.71
3 I1D	−0.00	−0.00	−0.00	2.52	2.74	3.19	−0.00	−0.00	−0.00	2.32	2.52	3.02
4 I2D	−0.00	−0.00	0.00	2.52	2.74	3.19	−0.01	−0.00	−0.00	2.38	2.55	2.93
5 I1D1	−0.00	0.00	−0.00	2.53	2.88	3.34	−0.00	−0.00	−0.00	2.32	2.69	3.11
6 I1D2	0.00	−0.00	−0.00	2.53	2.81	3.22	0.00	−0.00	−0.00	2.35	2.66	3.19
7 I2D1	0.00	0.00	−0.00	2.51	2.78	3.31	0.00	−0.00	−0.00	2.31	2.59	3.06
8 I2D2	−0.00	0.00	−0.00	2.62	2.79	3.28	−0.01	−0.00	−0.00	2.42	2.57	3.07

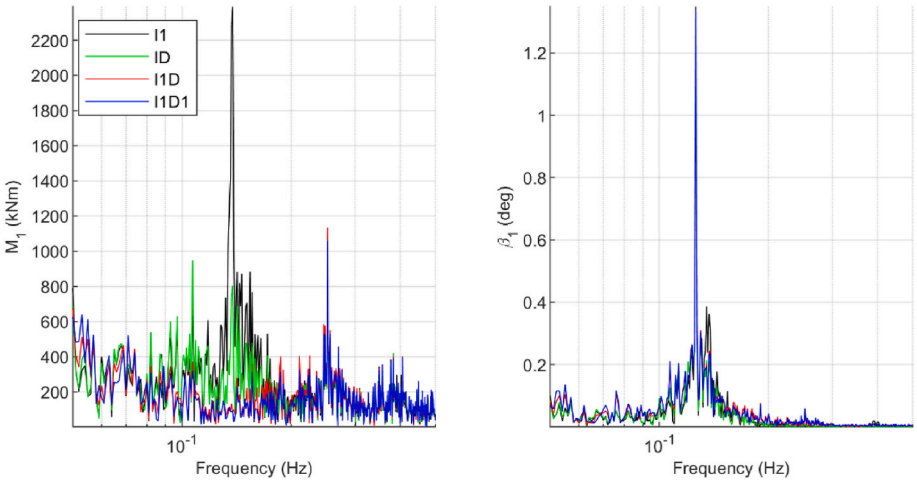

Fig. 11. Frequency domain response of the out-of-plane blade moment and pitch signal for blade 1 using Fourier spectra.

the evolution of the absolute value of the decoupling elements according to the implemented gain-scheduling strategy.

The analysis of the results in Table 6 shows that the proposed IPCs compared to the baseline obtain lower mean values of the M_t and M_y components, except for IPC2 ID, which presents slightly higher mean values of M_y than the baseline in case 3. In addition, all IPCs have lower STD values, which translates into lower DEL of the blade OoP moments. The mean values of the moments are 2 orders of magnitude smaller than the standard deviations. Fig. 10 shows that the proposed IPCs with inverted decoupling have a range of smaller oscillations of the M_t and M_y moments and higher pitch activity β_t and β_y. It should be noted that despite this higher activity in the non-rotational frame, this does not translate into higher actual pitch activity in the rotational frame, as observed from the $\overline{\text{NAT}}$ (β) values in Table 5. The IPC adaptive integral gains are in accordance with the calculations performed in the previous section. The IPC3 (I1D) shows higher integral gains than the IPC1 baseline. The IPC5 has even larger integral gains and considerably larger decoupling gains.

4.2.2. Frequency responses

Fig. 11 shows a frequency domain comparison of the IPCs selected in the previous section; specifically, it shows the Fourier spectrum of the out-of-plane bending moment (M_1) and pitch signal (β_1) of blade 1. IPCs 3 and 5 achieve a significant reduction of the main peak of the 1P component of the M_1 moment around the frequency of 0.126 Hz compared to the IPC1 baseline. As for the pitch signals, all three IPCs show similar peaks related to the 1P component, resulting in similar pitch signal effort.

5. Conclusions

The present study demonstrates that individual pitch control schemes with static inverted decoupling offer significant improvements in the mitigation of blade fatigue loads in large-capacity offshore wind turbines. The results highlight the following main findings.

- Reduction of fatigue loads: all proposed IPC schemes achieved a significant reduction in the damage equivalent load (DEL) of the out-of-plane blade moments compared to traditional IPC. In general, this improvement was achieved with a similar pitch actuator effort.
- Impact of static inverted decoupling: the IPC2 (ID) has shown that the simple inclusion of the inverted decoupling obtained from simple calculations to a previous decentralized IPC, without the need for optimization, already allows a reduction in the average DEL of the blade moments and the pitch control effort. It only requires readjusting the gains by multiplying them by a factor depending on the decoupling elements used. Therefore, this could be a very practical option to improve existing IPCs.
- Simplicity and adaptability: the optimized schemes IPC3 (I1D) and IPC5 (I1D1) offered the best compromise between simplicity and performance. IPC3 has one less parameter to optimize than IPC5, but IPC5 has a greater reduction in blade loads.
- Validation in large-capacity turbines: unlike many previous studies that focused on smaller-scale turbines, this work was carried out on a 15 MW reference turbine, providing crucial validation for the design and implementation of advanced control schemes in large-capacity turbines.

Future work will explore the extension of these strategies to floating turbines, where additional dynamics could benefit from inverted decoupling. Another point would be the integration of machine learning algorithms to dynamically tune the controller parameters in real time, further improving the operational efficiency. Overall, this work contributes to the development of advanced control technologies that improve the efficiency, durability, and sustainability of offshore wind turbines, aligning with global energy transition goals.

Data Availability Statement

The data presented in this study are openly available at https://zenodo.org/records/15471425.

CRediT authorship contribution statement

Manuel Lara: Writing – original draft, Visualization, Validation, Software, Methodology, Investigation, Data curation, Conceptualization. **Mario L. Ruz:** Writing – review & editing, Investigation, Funding acquisition. **Sebastiaan Paul Mulders:** Writing – review & editing, Supervision, Investigation. **Francisco Vázquez:** Writing – review & editing, Resources, Investigation. **Juan Garrido:** Writing – review & editing, Writing – original draft, Supervision, Investigation, Conceptualization, Visualization, Methodology, Funding acquisition.

Declaration of competing interest

The authors declare that they have no known competing financial interests or personal relationships that could have appeared to influence the work reported in this paper.

Acknowledgments

This research was funded by the Spanish Ministry of Science, Innovation and Universities (MCIU/AEI/10.13039/501100011033/FEDER, UE), grant number PID2023-149181OB-I00.

References

Aktan, H.D., Bottasso, C.L., 2023. Individual pitch control with a reduced actuator duty cycle. In: IEEE Conference on Control Technology and Applications (CCTA), pp. 581–586. https://doi.org/10.1109/CCTA54093.2023.10252554.

Abbas, N.J., Zalkind, D.S., Pao, L., Wright, A., 2022. A reference open-source controller for fixed and floating offshore wind turbines. Wind Energ. Sci. 7, 53–73. https://doi.org/10.5194/wes-7-53-2022.

Bonnie Jonkman, Rafael M. Mudafort, Andy Platt, E. Branlard, Mike Sprague, jjonkman, Hannah Ross, Hayman Consulting, Matt Hall, Ganesh Vijayakumar, Marshall Buhl, Pietro Bortolotti, Shreyas Ananthan, Michael S., Jon Rood, rdamiani, nrmendoza, sinolonghai, pschuenemann, … Alvaro Gonzalez Salcedo, 2023. OpenFAST/openfast: v3.4.1 (v3.4.1). Zenodo. https://doi.org/10.5281/zenodo.7632926.

Bossanyi, E.A., 2003. Individual blade pitch control for load reduction. Wind Energy 6 (2), 119–128. https://doi.org/10.1002/we.76.

Bossanyi, E.A., Fleming, P.A., Wright, A.D., 2013. Validation of individual pitch control by field tests on two-and three-bladed wind turbines. IEEE Trans. Control Syst. Technol. 21 (4), 1067–1078. https://doi.org/10.1109/TCST.2013.2258345.

Boukhezzar, B., Lupu, L., Siguerdidjane, H., Hand, M., 2007. Multivariable control strategy for variable speed, variable pitch wind turbines. Renew. Energy 32 (8), 1273–1287. https://doi.org/10.1016/j.renene.2006.06.010.

El Yaakoubi, A., Bouzem, A., El Alami, R., Chaibi, N., Bendaou, O., 2023. Wind turbines dynamics loads alleviation: overview of the active controls and the corresponding strategies. Ocean Eng. 278, 114070. https://doi.org/10.1016/j.oceaneng.2023.114070.

Energy, M.S., 2021. Leading innovation: MingYang smart energy launches MySE 16.0-242, the world's largest offshore hybrid drive wind turbine. Press release. MingYang Smart Energy. August 20, 2021.

Gaertner, E., et al., 2020. Definition of the IEA Wind 15-Megawatt Offshore Reference Wind Turbine Technical Report. *Technical Report NREL/TP-5000-75698*.

Gambier, A., 2022. Control of Large Wind Energy Systems. Springer. https://doi.org/10.1007/978-3-030-84895-8.

Garrido, J., Vázquez, F., Morilla, F., Hägglund, T., 2011. Practical advantages of inverted decoupling. Proc. IME J. Syst. Control Eng. 225 (7), 977–992. https://doi.org/10.1177/2041304110394556.

Geyler, M., Caselitz, P., 2008. Robust Multivariable Pitch Control Design for Load Reduction on Large Wind Turbines. https://doi.org/10.1115/1.2931510.

Goldberg, D.E., 1989. Genetic Algorithms in Search, Optimization, and Machine Learning. Addison-Wesley.

Goldberg, D.E., Deb, K., 1991. A comparative analysis of selection schemes used in genetic algorithms. Foundations of genetic algorithms, 1. Elsevier, pp. 69–93. https://doi.org/10.1016/B978-0-08-050684-5.50008-2.

Hägglund, T., Shinde, S., Theorin, A., Thomsen, U., 2022. An industrial control loop decoupler for process control applications. Control Eng. Pract. 123, 105138. https://doi.org/10.1016/j.conengprac.2022.105138.

Henry, A., Pusch, M., Pao, L., 2023. Modeling blade-pitch actuation power use in wind turbines. In: 2023 American Control Conference (ACC), pp. 1480–1485. https://doi.org/10.23919/ACC55779.2023.10156073.

I. IEC, 2005. 61400-1: Wind Turbines Part 1: Design Requirements, 177. International Electrotechnical Commission.

Jonkman, B.J., 2009. Turbsim User's Guide. https://doi.org/10.2172/965520. Golden, CO (United States), Version 1.50.

Kapasakalis, K.A., Gkikakis, A.E., Sapountzakis, E.J., Chatzi, E., Kampitsis, A.E., 2024. Multi-Objective Optimization of a Negative Stiffness Vibration Control System for Offshore Wind Turbines. https://doi.org/10.2139/ssrn.4715301.

Lara, M., Mulders, S.P., van Wingerden, J.-W., Vázquez, F., Garrido, J., 2023. Analysis of adaptive individual pitch control schemes for blade fatigue load reduction on a 15 MW wind turbine. Appl. Sci. 14 (1), 183. https://doi.org/10.3390/app14010183.

Lara, M., Vázquez, F., Garrido, J., 2024. Decentralized individual pitch control with inverted decoupling for wind turbines in the full load region. In: In: 2024 IEEE 19th Conference on Industrial Electronics and Applications (ICIEA), pp. 1–6. https://doi.org/10.1109/ICIEA61579.2024.10664980.

Lasheen, A., Elnaggar, M., Yassin, H., 2020. Adaptive control design and implementation for collective pitch in wind energy conversion systems. ISA Trans. 102, 251–263. https://doi.org/10.1016/j.isatra.2019.11.019.

Minh Le, L., Van Nguyen, D., Chang, S., Kim, D., Cho, S.G., Nguyen, D.D., 2019. Vibration control of jacket offshore wind turbine subjected to earthquake excitations by using friction damper. Journal of Structural Integrity and Maintenance 4 (1), 1–5. https://doi.org/10.1080/24705314.2019.1565055.

MLife wind research NREL. Accessed: February. 17, 2025. [Online]. Available: https://www.nrel.gov/wind/nwtc/mlife.html.

Mulders, S.P., Pamososuryo, A.K., Disario, G.E., van Wingerden, J.-W., 2019. Analysis and optimal individual pitch control decoupling by inclusion of an azimuth offset in the multiblade coordinate transformation. Wind Energy 22 (3), 341–359. https://doi.org/10.1002/we.2289.

Mulders, S., Pamososuryo, A., van Wingerden, J., 2020. Efficient tuning of individual pitch control: a bayesian optimization machine learning approach. J Phys Conf Ser 1618 (2), 022039. https://doi.org/10.1088/1742-6596/1618/2/022039.

Muñoz-Palomeque, E., Sierra-García, J.E., Santos, M., 2024. Técnicas de control inteligente para el seguimiento del punto de máxima potencia en turbinas eólicas. Revista Iberoamericana de Automática e Informática industrial 21 (3), 193–204. https://doi.org/10.4995/RIAI.2024.21097.

Musial, W., Spitsen, P., Duffy, P., Beiter, P., Shields, M., Mulas, H.D., Hammond, R., Marquis, M., King, J., Sathish, S., 2023. Offshore Wind Market Report. 2023 Edition, Golden, CO (United States). https://doi.org/10.2172/2001112.

Natarajan, A., 2022. Damage equivalent load synthesis and stochastic extrapolation for fatigue life validation. Wind Energy Science 7 (3), 1171–1181. https://doi.org/10.5194/wes-7-1171-2022.

Niranjan, R., Ramisetti, S.B., 2022. Insights from detailed numerical investigation of 15 MW offshore semi-submersible wind turbine using aero-hydro-servo-elastic code. Ocean Eng. 251, 111024. https://doi.org/10.1016/j.oceaneng.2022.111024.

Patro, S.R., Panda, S., Ramana, G., Banerjee, A., 2024. Optimal multiple tuned mass dampers for monopile supported offshore wind turbines using genetic algorithm. Ocean Eng. 298, 117356. https://doi.org/10.1016/j.oceaneng.2024.117356.

Ragan, P., Manuel, L., 2007. Comparing estimates of wind turbine fatigue loads using time-domain and spectral methods. Wind Eng. 31 (2), 83–99. https://doi.org/10.1260/030952407781494494.

Rasekh, S., Aliabadi, S.K., 2023. Toward improving the performance of a variable pitch vertical axis wind turbine (VP-VAWT), part 2: multi-Objective optimization using NSGA-II with CFD in the loop. Ocean Eng. 278, 114308. https://doi.org/10.1016/j.oceaneng.2023.114308.

Routray, A., Sivakumar, N., Hur, S., Bang, D., 2023. A comparative study of optimal individual pitch control methods. Sustainability 15 (14), 10933. https://doi.org/10.3390/su151410933.

Serrano, C., Sierra-Garcia, J.-E., Santos, M., 2022. Hybrid optimized fuzzy pitch controller of a floating wind turbine with fatigue analysis. J. Mar. Sci. Eng. 10 (11), 1769. https://doi.org/10.3390/jmse10111769.

Ungurán, R., Petrović, V., Boersma, S., van Wingerden, J.-W., Pao, L.Y., Kühn, M., 2019. Feedback-feedforward individual pitch control design for wind turbines with uncertain measurements. In: 2019 American Control Conference (ACC), pp. 4151–4158. https://doi.org/10.23919/ACC.2019.8814757.

Vali, M., van Wingerden, J.-W., Kühn, M., 2016. Optimal multivariable individual pitch control for load reduction of large wind turbines. In: 2016 American Control Conference (ACC), pp. 3163–3169. https://doi.org/10.1109/ACC.2016.7525404.

Van Engelen, T.G., 2006. Design Model and Load Reduction Assessment for multi-rotational Mode Individual Pitch Control (Higher Harmonics Control).

Veers, P., Bottasso, C.L., Manuel, L., Naughton, J., Pao, L., Paquette, J., Robertson, A., Robinson, M., Ananthan, S., Barlas, T., Bianchini, A., Bredmose, H., Horcas, S.G., Keller, J., Madsen, H.A., Manwell, J., Moriarty, P., Nolet, S., Rinker, J., 2023. Grand challenges in the design, manufacture, and operation of future wind turbine systems. Wind Energ. Sci. 8, 1071–1131. https://doi.org/10.5194/wes-8-1071-2023.

Williams, R., Zhao, F., 2023. Global Offshore Wind Report, pp. 118–2023.

Wu, F., Zhang, X.-P., Ju, P., Sterling, M.J.H., 2008. Decentralized nonlinear control of wind turbine with doubly fed induction generator. IEEE Trans. Power Syst. 23 (2), 613–621. https://doi.org/10.1109/TPWRS.2008.920073.

Yang, X., Xu, L., Liu, Y., Xu, D., 2007. Multivariable predictive functional control for doubly fed induction generator. In: IEEE International Conference on Control and Automation, pp. 80–83. https://doi.org/10.1109/ICCA.2007.4376322.

Yuan, Y., Chen, X., Tang, J., 2020. Multivariable robust blade pitch control design to reject periodic loads on wind turbines. Renew. Energy 146, 329–341. https://doi.org/10.1016/j.renene.2019.06.136.